J Nanopart Res (2013) 15:1842
DOI 10.1007/s11051-013-1842-8

RESEARCH PAPER

Automatic determination of the size of elliptical nanoparticles from AFM images

Jiří Sedlář · Barbara Zitová · Jaromír Kopeček · Jan Flusser · Tatiana Todorciuc · Irena Kratochvílová

Received: 17 March 2013 / Accepted: 5 July 2013

Abstract The objective of this work was to develop an accurate method for automatic determination of the size of elliptical nanoparticles from atomic force microscopy (AFM) images that would yield results consistent with results of manual measurements by experts. The proposed method was applied on phenylpyridyldiketopyrrolopyrrole (PPDP), a granular organic material with a wide scale of application and highly sensitive particle-size properties. A PPDP layer consists of similarly sized elliptical particles (c. 100 nm × 50 nm) and its properties can be estimated from the average length and width of the particles. The developed method is based on segmentation of salient particles by the watershed transform and approximation of their shapes by ellipses computed by image moments; it estimates the lengths and widths of the particles by the major and minor axes, respectively, of the corresponding ellipses. Its results proved to be consistent with results of manual measurements by a trained expert. The comparison showed that the developed method could be used in practice for precise automatic measurement of PPDP particles in AFM images.

Keywords Atomic force microscopy · Image moments · Pyrrole derivatives · Size determination · Watershed segmentation

J. Sedlář (✉) · B. Zitová · J. Flusser
Institute of Information Theory and Automation, Academy of Sciences of the Czech Republic, Pod Vodárenskou věží 4, 182 08 Prague 8, Czech Republic
e-mail: sedlar@utia.cas.cz

J. Kopeček · I. Kratochvílová
Institute of Physics, Academy of Sciences of the Czech Republic, Na Slovance 2, 182 21 Prague 8, Czech Republic

T. Todorciuc
Faculty of Chemical Engineering and Environmental Protection, Gheorghe Asachi Technical University, Mangeron Bvd. 71, 700050 Iasi, Romania

Introduction

Nanoparticle size determination is a fundamental step in analysis of nanomaterials since the size of nanoparticles has a large impact on various practically important material properties, e.g. conductivity, optical transparency, and biocompatibility. For a majority of nanomaterials, fast and precise determination of nanoparticle sizes is a crucial task. In this paper we present a new method meeting contemporary demands—automatic and accurate determination of nanoparticle sizes from atomic force microscopy (AFM) images. The method is applied on phenylpyridyldiketopyrrolopyrrole (PPDP), a granular organic material with a wide scale of application and highly sensitive particle-size properties.

PPDP as organic molecular compounds with aromatic and heterocyclic ring in the structure has unique

Published online: 24 July 2013

properties concerning conductivity, photoconductivity, optical and photochromatic effects, and, in some cases, also conformation changes caused by the charge transport and shift. PPDP layers consist of mostly spatially separated ellipsoidal particles; their topography can be observed by AFM (see Fig. 1). Accurate determination of the size of PPDP clusters is crucial for practical purposes. Material conductivity in sensors, for example, strongly depends on particle sizes (Mizuguchi et al. 2006; Salyk et al. 2010). And for applications of PPDP as very good working organic pigments, the size of particles is one of the most important parameters for a proper technology setting (Gangopadhyay and Molla 2011; Qu and Tian 2012; Song et al. 2007). Currently used manual measurement of PPDP particles in AFM images is laborious and time-consuming. The objective of this work was to develop an accurate method that would determine the size of salient PPDP particles from AFM images automatically and consistently with manual measurements by a trained expert.

The atomic force microscope (Binnig et al. 1986) is an imaging device that allows measurement of the topography of solid body surfaces with very high resolution. It gradually moves an elastic cantilever with a sharp tip close above the surface. The surface applies the interactive force to the tip, which deflects the cantilever. The measured deflection estimates the height of the surface (Mironov 2004). AFM thus allows measurement of the topography without damage to the scanned surface.

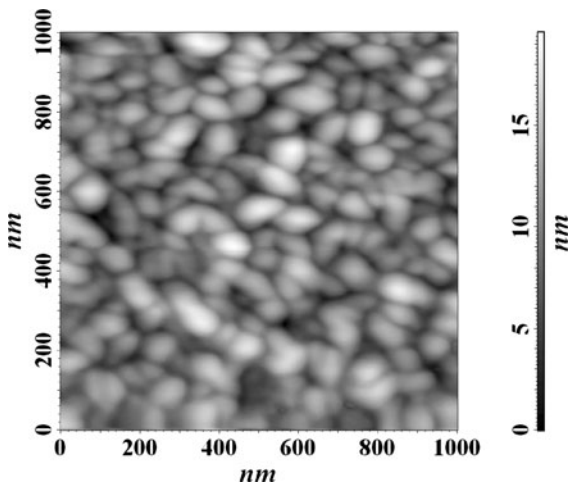

Fig. 1 Atomic force microscopy (AFM) image of a phenylpyridyldiketopyrrolopyrrole (PPDP) sample. The resolution of the image (256 × 256 pixels) and the size of the scanned area (1,000 nm × 1,000 nm) correspond to approximate spatial resolution of 3.9 nm per pixel. The measured height ranges from 0 nm (*black*) to 19.6 nm (*white*)

AFM images represent just an approximation of the scanned topography. The observed image is, in fact, a convolution between the contacting tip and the surface of the sample (Villarrubia 1997). As a result, only details larger than the diameter of the tip are observed. However, the exact shape of the tip is unknown; it can even change during measurement, particularly due to breaking or due to adhesion of dust particles or parts of the sample. Furthermore, AFM images typically contain noise artifacts (Mironov 2004). Analysis of AFM images should account for these distortions and compensate for them using prior information about the scanned sample.

The objective of this work was to automatically determine the size of PPDP particles in AFM images. PPDP samples consist of similarly sized ellipsoidal particles, so the size of each particle can be characterized by its length and width, and the size of particles in an image can be characterized by their average size. Researchers thus usually measure only a representative subset of particles and compute just their average length and width.

Currently used manual measurement of PPDP particles in AFM images is problematic. The images typically contain hundreds to thousands of particles, which makes manual measurements time-consuming and laborious. Therefore in practice researchers measure only a relatively small number of particles to estimate the average length and width. This fact, along with the error of manual analysis, decreases accuracy and consistency of results.

Automation of the measurement process would not only speed up the evaluation of AFM images but it could also increase the accuracy and consistency of results. Firstly, it would eliminate errors introduced by human operators. And secondly, it could use a higher number of particles to estimate the average length and width. Development of such an automatic method is thus of great interest.

Existing methods for automatic analysis of AFM images are not appropriate for accurate determination of PPDP particle sizes. Methods for surface reconstruction in AFM images (Villarrubia 1997) do not utilize prior information about the shape of scanned surface. Existing methods for measurement of

particles in AFM images are not convenient for mostly spatially separated particles such as PPDP because the methods are sensitive to high-frequency noise (Toman 2001) or designed specifically for densely packed particles (Fekete et al. 2012).

This paper introduces a new automatic method that enables accurate size determination of mostly spatially separated ellipsoidal particles from AFM images. The method is based on rough segmentation of particles by the watershed transform and approximation of their shapes by ellipses; it computes parameters of the approximating ellipses by image moments. The method estimates the length and width of salient particles by the major and minor axes, respectively, of the approximating ellipses. It excludes partially occluded or otherwise distorted particles from measurements since they cannot be measured with sufficient accuracy. The use of prior information about the elliptical shape of the analyzed particles increases robustness of the method to distortions in AFM images.

The rest of this paper is organized as follows: "Mathematical background" section explains the basics of image moments; "Method" section describes in detail the proposed method; "Results" section compares results of the automatic method with results of manual measurements; "Discussion" section discusses the results and outlines possible applications of the developed method; and "Conclusion" section concludes this paper.

Mathematical background

This section describes the basics of image moments (Flusser et al. 2009), which the developed method utilizes for approximation of particle shapes by ellipses (see "Approximation by ellipses" subsection).

Image moments are projections of a grayscale image function $f : \mathbb{R}^2 \to \mathbb{R}$, i.e. a finite piece-wise continuous real function of two variables $(x, y) \in \mathbb{R}^2$ with a compact support $D \subset \mathbb{R}^2$, to polynomial bases. They have a number of applications in image processing, particularly in object recognition and representation.

Geometric moment

$$m_{pq} = \iint_D f(x,y) x^p y^q dxdy,$$

where $p, q \in \mathbb{N}_0$, is a projection of image function f with compact support D onto the basis $\{x^p, y^q\}$, where $(p + q)$ is the order of the moment. Zero-order moment m_{00} equals the volume of f and $x_t = m_{10}/m_{00}$ and $y_t = m_{01}/m_{00}$ are coordinates of its centroid; translation of the image by vector $(-x_t, -y_t)$ centers the image in zero.

Central geometric moment

$$\mu_{pq} = \iint_D f(x,y)(x - x_t)^p (y - y_t)^q dxdy$$

of order $(p + q)$ equals the geometric moment m_{pq} for a centered image; it is thus invariant to translation of image f. Central moments μ_{20} and μ_{02} represent the variance of f in axes x and y, respectively, and central moment μ_{11} represents the co-variance between them.

A normalized position of image f is acquired by rotation of the centered image around zero by angle

$$\alpha = \frac{1}{2} \arctan\left(\frac{2\mu_{11}}{\mu_{20} - \mu_{02}}\right), \quad \mu_{11} \neq 0 \vee \mu_{20} \neq \mu_{02};$$

if $\mu_{11} = 0$ and $\mu_{20} = \mu_{02}$, the image is already in a normalized position. Ambiguity of the normalized position can be removed by flipping the rotated image horizontally or vertically to satisfy conditions $\mu'_{20} \geq \mu'_{02}$ and $\mu'_{30} \geq 0$, for example. Second order moments of an image in a normalized position satisfy conditions $\mu'_{11} = 0$ and $\mu'_{20} \geq \mu'_{02}$. Their values can be expressed as

$$\mu'_{20} = \frac{1}{2}\left(\mu_{20} + \mu_{02} + \sqrt{(\mu_{20} - \mu_{02})^2 + 4\mu_{11}^2}\right),$$
$$\mu'_{02} = \frac{1}{2}\left(\mu_{20} + \mu_{02} - \sqrt{(\mu_{20} - \mu_{02})^2 + 4\mu_{11}^2}\right).$$

A reference ellipse of image f in a normalized position is an ellipse

$$\frac{x^2}{a_{\text{ref}}^2} + \frac{y^2}{b_{\text{ref}}^2} \leq 1, \quad a_{\text{ref}} \geq b_{\text{ref}} > 0,$$

with the same image moments μ_{pq} as image moments of f up to order two, i.e. $(p + q) \leq 2$; a_{ref} and b_{ref} denote its major and minor semiaxes, respectively.

Method

The objective of the proposed method is computation of the average length and width of salient particles in AFM images of PPDP samples. AFM images are grayscale images with pixel values linearly

corresponding to the measured height of the scanned surface (see Fig. 1); let f denote the image function and D its support.

The method is based on two assumptions. Firstly, each image contains similarly sized particles. This means that the average size of particles in an image can be estimated with low error by the average size of a subset of particles. Secondly, the particles are ellipsoidal. Their shapes can thus be approximated by ellipses and their lengths and widths can be estimated by the corresponding major and minor axes, respectively. The assumptions follow from known physical properties of PPDP samples.

The developed method consists of the following steps (see Fig. 2): first, it reduces high-frequency noise in the AFM image; then it segments the denoised image by watershed transform and excludes regions containing noise artifacts or partly occluded particles; in the retained regions, the method approximates the shapes of particles by ellipses; it approximates the topography of each particle by the upper half of an ellipsoid and excludes particles that significantly differ from the corresponding ellipsoids; finally, it estimates the average length and width of particles in the image by the average lengths of the major and minor axes, respectively, of the retained approximating ellipses. The rest of this section describes the steps in greater detail.

Denoising

The method first reduces high-frequency noise in the AFM image. It convolves the image with a radially symmetric Gaussian kernel

$$h(x,y) = h(r) = \frac{1}{\sqrt{2\pi}\sigma} e^{-\frac{r^2}{2\sigma^2}},$$

where σ is the standard deviation of the Gaussian and $r = (x^2 + y^2)^{\frac{1}{2}}$ the distance from the center of the kernel. The Gaussian low pass filter proved sufficient for suppression of high-frequency AFM noise. Moreover, it smooths the image function, and thus avoids oversegmentation in the next step of the method.

Segmentation

The method then segments the denoised image into regions corresponding to separate particles and removes regions that are inappropriate for measurement.

The method segments the denoised image by the watershed transform by immersion (Vincent and Soille 1991) (see Fig. 3a). Although the segmentation may not separate some overlapping particles—the method addresses this problem later—a vast majority of watershed regions contain exactly one particle. Note that a watershed transform of the original AFM image without smoothing would lead to oversegmentation, with watershed lines dividing many particles into multiple regions.

The method then detects watershed regions with particles inappropriate for measurements and excludes them from further processing. This includes regions containing AFM noise artifacts or partly occluded particles. For this purpose, the method estimates central parts (cores) of particles. It locally normalizes brightness in each region D_i $(i = 1, \ldots, n)$ of the denoised image f to

$$f_{\mathrm{norm}}(x,y) = f(x,y) + (\max_{D} f - \max_{D_i} f), \quad (x,y) \in D_i,$$

where $D = \bigcup_{i=1}^{n} D_i$ is the domain of f and n is the number of watershed regions (see Fig. 3b). Then it segments the normalized image f_{norm} by thresholding (see Fig. 3c) with a convenient global threshold t_0. Note that this approach is equivalent to local thresholding with region-specific thresholds. Regions with cores adjacent to watershed lines or image borders (see Fig. 3c) correspond to AFM noise artifacts or particles partly occluded by neighboring particles or to particles partly cropped by image borders, respectively. The method excludes such regions from further processing (see Fig. 3d).

Approximation by ellipses

The method approximates the shapes of particles in the retained regions by ellipses (see Fig. 4a). It approximates the shape of each particle by an ellipse

$$\frac{x^2}{a^2} + \frac{y^2}{b^2} \leq 1, \quad a \geq b > 0,$$

with major and minor semiaxes

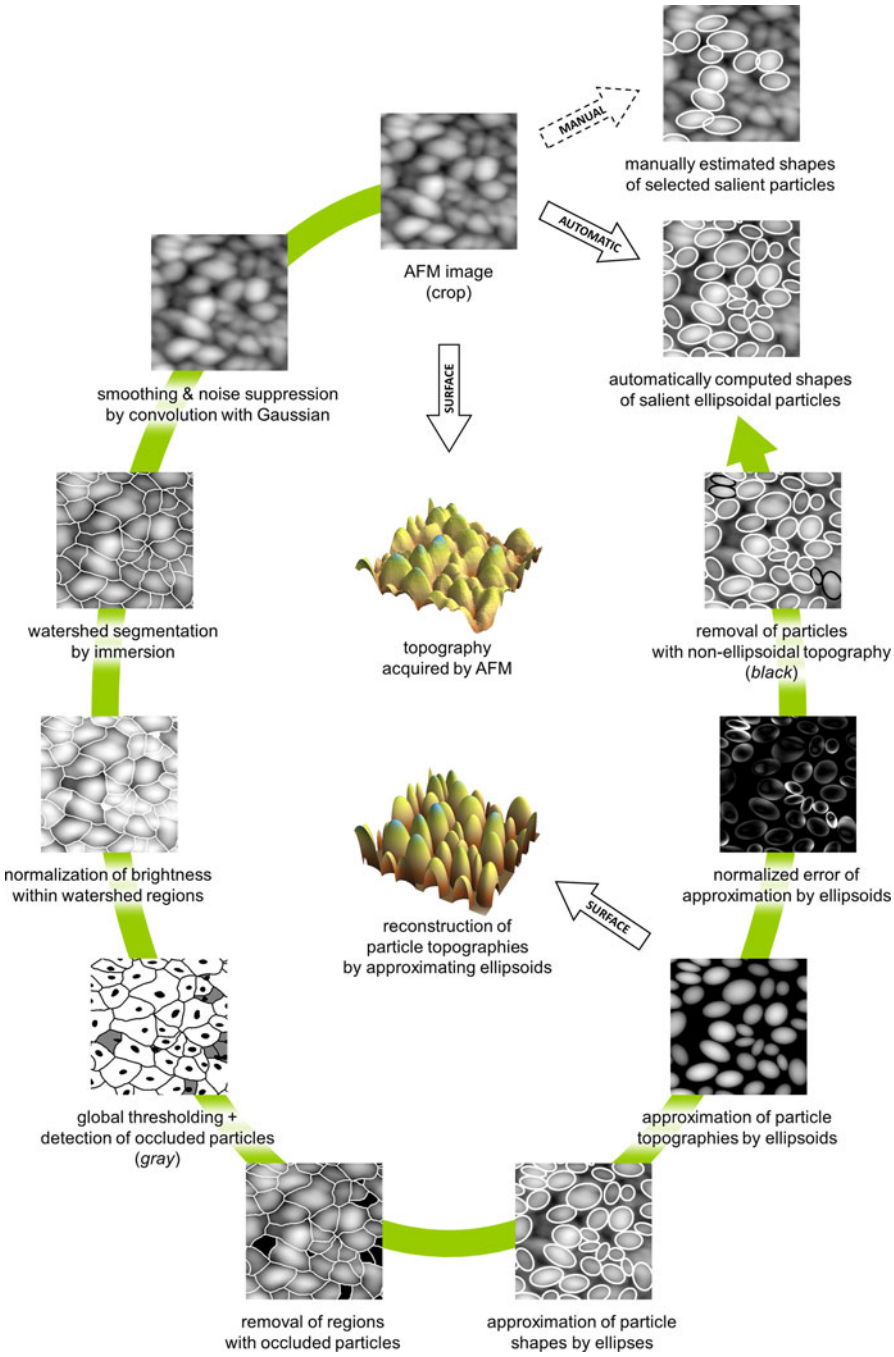

Fig. 2 Steps of the developed method for automatic measurement of ellipsoidal particles in AFM images

$$a = 2\sqrt{\mu'_{20}}, \quad b = 2\sqrt{\mu'_{02}}$$

defined by image moments μ'_{20} and μ'_{02}, respectively, of the denoised image f within region D_i $(i = 1, \ldots, n)$ in the normalized position (see "Mathematical background" section). The major axis $2a$ and minor axis $2b$ of the approximating ellipse estimate the length and width, respectively, of the particle. This approximation is based on the concept of the reference ellipse.

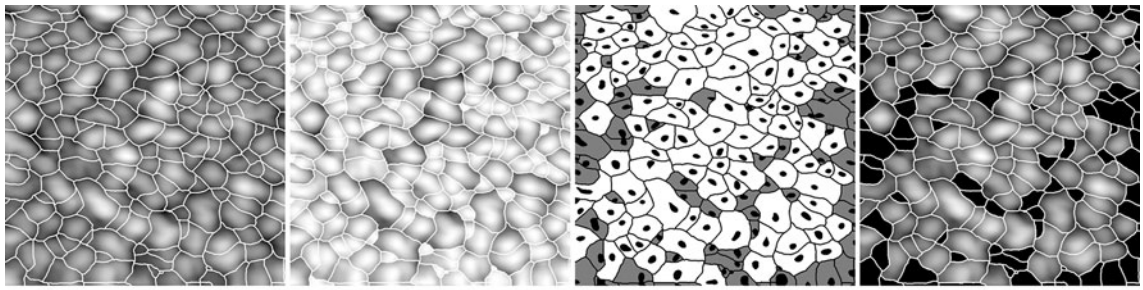

Fig. 3 **a** Segmentation of the denoised AFM image by watershed transform by immersion. **b** Local normalization of brightness within watershed regions. **c** Global thresholding of the normalized regions; regions with cores adjacent to the watershed lines or image borders (*gray*) correspond to noise artifacts or partly occluded particles. **d** Removal of watershed regions with cores adjacent to the watershed lines or image borders

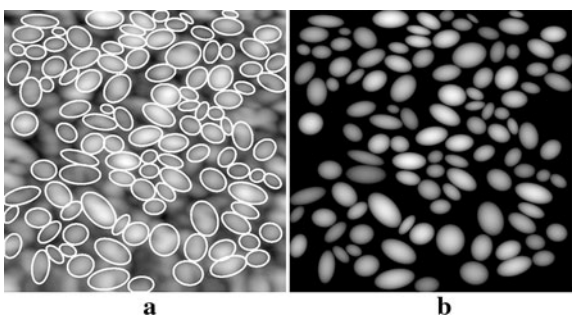

Fig. 4 **a** Approximation of particles shapes by ellipses. **b** Approximation of particles topographies by ellipsoids

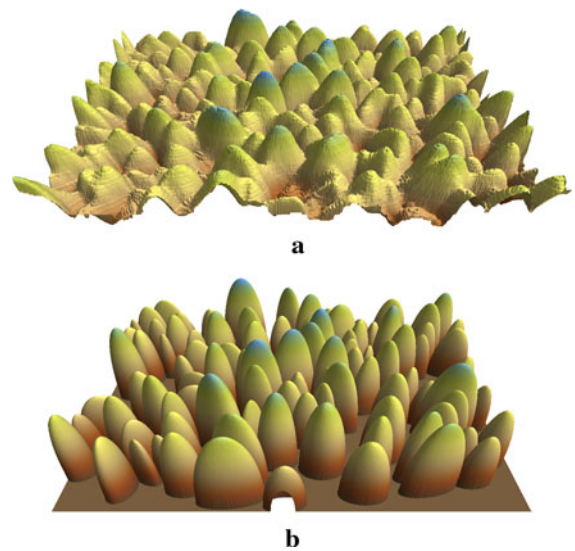

Fig. 5 **a** Topography of a PPDP sample acquired by AFM. **b** Reconstruction of topographies of salient PPDP particles by approximating ellipsoids

Approximation by ellipsoids

The method then detects non-ellipsoidal particles and excludes them from measurement. It approximates topographies of the detected particles by ellipsoids (see Fig. 5) and computes the approximation error. The error is high for overlapping or tilted particles; the method cannot measure such particles with sufficient precision.

The method constructs the upper half of an ellipsoid

$$\frac{x^2}{a^2}+\frac{y^2}{b^2}+\frac{z^2}{c^2}=1, \quad a,b,c>0 \quad \& \quad z\geq 0$$

above each approximating ellipse. The semiaxes a and b equal the major and minor semiaxes, respectively, of the approximating ellipse. The method estimates the length of the semiaxis c, which is perpendicular to the image plane, as

$$c=f(x_t,y_t),$$

where (x_t, y_t) is the center of the approximating ellipse. The height of the approximating ellipsoid

$$z(x,y)=\begin{cases} c\left(1-\left(\frac{x^2}{a^2}+\frac{y^2}{b^2}\right)\right)^{\frac{1}{2}}, & \frac{x^2}{a^2}+\frac{y^2}{b^2}\leq 1, \\ 0, & \text{otherwise} \end{cases}$$

approximates the brightness function of the denoised image within the domain of the approximating ellipse (see Fig. 4b).

The method then measures the dissimilarity between the surface of the particle and the approximating ellipsoid. It defines the approximation error as

$$\varepsilon = \frac{\iint_D (z(x,y))^2 (f(x,y) - z(x,y))^2 \, dxdy}{\iint_D (z(x,y))^2 \, dxdy}, \quad (1)$$

where f is the brightness function of the denoised image and D is the domain of the approximating ellipse. The weights $(z(x,y))^2$ suppress the influence of outer parts of the approximation ellipse, which are usually distorted by the convolution of neighboring particles with the cantilever tip. The approximation error is a measure of the difference between the surface of the particle and its approximating ellipsoid: the lower the approximation error is, the closer the surface of the particle matches the approximating ellipsoid. The method excludes particles with approximation errors

$$\varepsilon > \varepsilon_0,$$

where ε_0 is an appropriate threshold, from measurements because they would decrease accuracy of the computed results.

Measurement

Finally, the method estimates the average length and width of all particles in the AFM image by the average length and width, respectively, of the retained particles. The method estimates their lengths and widths (see Fig. 7) by the lengths of the major and minor axes $2a$ and $2b$, respectively, of the corresponding approximating ellipses (see Fig. 6a).

Results

Performance of the proposed method was tested on a set of 11 AFM images of PPDP samples. The PPDP compound was prepared by reaction of pyrrolinone ester with corresponding nitrile (Vyňuchal et al. 2008). Thin films of PPDP were prepared by a vacuum evaporation method. The deposition of the active PPDP layer was carried out in a vacuum coating facility with an ultimate pressure of 1×10^{-4} Pa pumped by a diffusion oil pump. Thin films of thickness 100 nm were deposited on selected substrates (Salyk et al. 2010). The samples were scanned by the NTEGRA Prima apparatus (NTEGRA Prima (NT-MDT)) manufactured by NT-MDT (NT-MDT, Russian Federation) using the semi-contact (tapping) mode (Mironov 2004) in order to avoid damage of the soft organic material, and the NSG01 tip (NSG01 (NT-MDT)) with guaranteed curvature radius of 10 nm. The samples were scanned with approximate spatial resolution of 3.9 nm per pixel; the size of the scanned area was 1,000 nm × 1,000 nm and the resolution of the AFM images was 256 × 256 pixels.

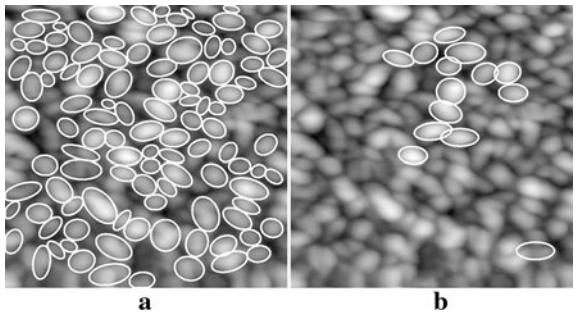

Fig. 6 **a** Automatically computed shapes of salient ellipsoidal particles. **b** Manually estimated shapes of particles selected for measurement

The acquired images were artificially colored by the AFM imaging software for easier visual evaluation; note that AFM images contain information only about the height of surface, however. For purposes of automatic evaluation, the color images were transformed to grayscale by mapping the 256-level color scale to a 256-level gray scale, with pixel values scaled to [0,1] interval.

Automatic measurement of particle sizes in the grayscale AFM images was performed by the proposed method (see Fig. 2). In each image, the method detected salient particles and estimated their average lengths and widths in pixels. The global threshold t_0 for computation of cores in watershed regions was set to $t_0 = 0.97$. Cores on watershed lines and image borders were detected by standard morphological operations, namely binary dilation with a 3×3 structural element. The approximation error threshold was set to $\varepsilon_0 = 0.015$.

For purposes of comparison, four of the testing AFM images were measured manually by a researcher. Based on his knowledge and experience, he selected particles convenient for measurement and approximated their shapes by ellipses (see Fig. 6b) so that the major and minor axes corresponded to the lengths and widths of the particles. In each image he selected and measured only a relatively small number of particles that he considered sufficient for estimation

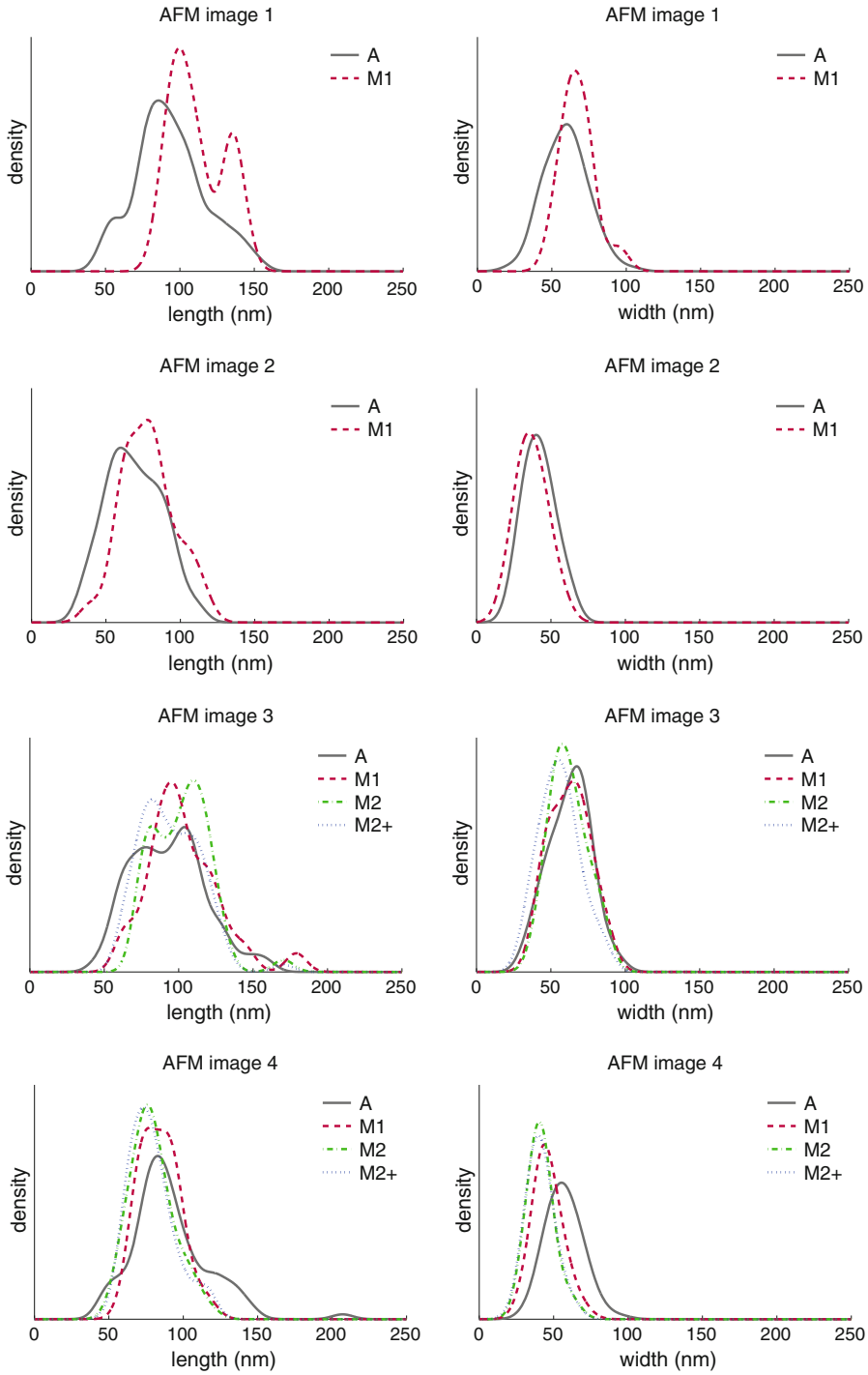

Fig. 7 Automatically and manually estimated densities of the lengths (*left*) and widths (*right*) of PPDP particles in four AFM images. Curve "A" (*solid*) corresponds to the automatic measurement, curves "M1" (*dashed*) and "M2" (*dash-dot*) to the first and second manual measurements, respectively, and curve "$M2^{+}$" (*dotted*) to the second measurement with additionally measured particles (see "Results" section)

of the average length and width of all particles in the image with low error. He measured two of these images again, this time in two phases: in the first phase, as before, he selected for measurement a small number of salient particles; in the second phase, he added further salient particles that he considered also convenient for measurement.

Results of the automatic and manual measurements were compared by estimates of the densities of the lengths and widths of particles in each image (see

Fig. 7). The density estimates were computed from the measured values by convolution with a Gaussian kernel with standard deviation 5 pixels. The results were further compared by the following two statistics. The first one measured the consistency in detection, namely the ratio of the number of particles selected by both automatic and manual measurements to the number of particles selected only manually (see Table 1). The second statistic measured the Dice similarity coefficient (DSC) (Crum et al. 2006; Dice 1945), a widely used measure of agreement between two segmentation methods. It ranges from zero to one, corresponding to no and full overlap, respectively, of two segmented shapes. It is defined as

$$\mathrm{DSC(A,M)} = \frac{1}{n}\sum_{i=1}^{n}\frac{2|A_i \cap M_i|}{|A_i| + |M_i|}, \qquad (2)$$

where n denotes the number of particles that were measured by both methods, A_i denotes the automatically computed shape of the particle i, M_i the manually measured shape of the same particle, and $|\cdot|$ denotes the area of the shape (see Table 1); note that the coefficient considers only particles measured by both methods. For computation of these comparative statistics, two ellipses from different measurements were attributed to the same particle if their centers lay within each other's shape.

Table 1 Comparison of automatic and manual measurements

Image	Method X	Method Y	|X&Y|/|Y| (%)	DSC(X,Y)
1	A	M1	100	0.84
2	A	M1	58	0.76
3	A	M1	90	0.83
3	A	M2	89	0.82
3	A	$M2^+$	79	0.81
3	M2	M1	93	0.84
3	$M2^+$	M1	100	0.84
4	A	M1	66	0.76
4	A	M2	72	0.71
4	A	$M2^+$	73	0.72
4	M2	M1	63	0.83
4	$M2^+$	M1	89	0.80

Method "A" denotes the automatic measurement, methods "M1" and "M2" denote the first and second manual measurement sessions, respectively, and method "$M2^+$" denotes the second session with additionally measured particles (see "Results" section). Column "|X&Y|/|Y|" denotes the ratio of the number of particles selected by both measurements X and Y to the number of particles selected by measurement Y; column "DSC(X,Y)" denotes the Dice similarity coefficient (see Eq. (4.1)) for methods X and Y

Discussion

In order to evaluate performance of the developed automatic method, its results were compared with results of the manual measurements. The measurement results could not be compared with the true lengths and widths of particles due to limitations of AFM, namely convolution of the scanned surface with the contacting tip (see "Introduction" section). The automatically and manually measured values are both just estimates of the real lengths and widths of particles, and thus only consistency between the automatic and manual measurements could be evaluated.

The estimated densities of the lengths and widths of particles in the AFM images (see Fig. 7) illustrate close similarity between results of the automatic and manual measurements. The comparative statistics (see Table 1) showed that while the automatic method did not measure some manually measured particles, the overlap of automatically and manually estimated shapes was comparable to the overlap of shapes estimated by different manual measurements. Such results indicate that the automatic method could be used in place of manual measurements.

Although the method was primarily developed for measurements in physics, it can be also applied to measurement of morphologically similar data in biology and medicine. The method could be used, for example, for measurement of ellipsoidal microorganisms or elliptical cells (Cloppet and Boucher 2010), for example.

Conclusion

This paper has introduced a new method for automatic determination of the size of phenylpyridyldiketopyrrolopyrrole (PPDP) particles from atomic force microscopy (AFM) images. The method assumes that the images contain similarly sized elliptical particles. It is based on segmentation by the watershed transform and approximation of particles by ellipses computed by image moments; the length and width of each

particle are estimated by the major and minor axes, respectively, of the corresponding approximating ellipse. The main advantage of the proposed method is its robustness to partial overlaps of particles and to high-frequency noise in AFM images. Its performance was tested on AFM images of PPDP samples and its results compared with results of manual measurements. The comparisons showed consistency between the measurements and indicated that the developed method could be used in practice for precise automatic measurement of elliptical nanoparticles in AFM images.

Acknowledgments This work was partly supported by the Czech Science Foundation Grants No. GAP103/11/1552 and GAP304/10/1951, and by the Technological Agency of the Czech Republic Grant No. TA01011165.

References

Binnig G, Quate CF, Gerber C (1986) Atomic force microscope. Phys Rev Lett 56(9):930–933. doi:10.1103/PhysRevLett.56.930

Cloppet F, Boucher A (2010) Segmentation of complex nucleus configurations in biological images. Pattern Recogn Lett 31(8):755–761. doi:10.1016/j.patrec.2010.01.022

Crum WR, Camara O, Hill DLG (2006) Generalized overlap measures for evaluation and validation in medical image analysis. IEEE Trans Med Imaging 25(11):1451–1461. doi:10.1109/TMI.2006.880587

Dice LR (1945) Measures of the amount of ecologic association between species. Ecology 26:297–302

Fekete L, Kůsová K, Petrák V, Kratochvílová I (2012) AFM topographies of densely packed nanoparticles: a quick way to determine the lateral size distribution by autocorrelation function analysis. J Nanoparticle Res 14(8):1–10. doi:10.1007/s11051-012-1062-7

Flusser J, Suk T, Zitová B (2009) Moments and moment invariants in pattern recognition. Wiley, Chichester

Gangopadhyay R, Molla MR (2011) Polypyrrole–polyvinyl alcohol stable nanodispersion: a prospective conducting black ink. J Polym Sci B: Polym Phys 49(11):792–800. doi:10.1002/polb.22216

Mironov VL (2004) Fundamentals of scanning probe microscopy. Russian Academy of Sciences, Institute for Physics of Microstructures, Nizhniy Novgorod, URL http://physics.gu.se/popok/SPM/Mironov.pdf

Mizuguchi J, Imoda T, Takahashi H, Yamamaki H (2006) Polymorph of 1,4-diketo-3,6-bis-(4′-dipyridyl)-pyrrolo-[3,4-c]pyrrole and their hydrogen bond network: A material for H_2 gas sensor. Dyes Pigment 68(1):47–52. doi:10.1016/j.dyepig.2005.01.001

NSG01 (NT-MDT) URL http://ntmdt-tips.com/products/view/nsg01

NTEGRA Prima (NT-MDT) URL http://www.ntmdt.com/modular-afm/prima

NT-MDT (1998-2013) URL http://www.ntmdt.com/

Qu S, Tian H (2012) Diketopyrrolopyrrole (DPP)-based materials for organic photovoltaics. Chem Commun 48(25):3039–3051. doi:10.1039/C2CC17886A

Salyk O, Vyňuchal J, Kratochvílová I, Todorciuc T, Pavluch J, Toman P (2010) Study of phenylpyridyldiketopyrrolopyrrole interaction with hydrogen in gas and in acids. Dyes Pigment 207(10):2327–2333. doi:10.1002/pssa.200925535

Song KT, Cho SH, Lee JY (2007) Conjugated polymers: theory, synthesis, properties, and characterization, 3rd edn. CRC Press, Boca Raton, chap Recent Advances in Polypyrrole, pp 8–1–8–87. Handbook of Conducting Polymers

Toman M (2001) Analýza STM snímků pořízených elektronovým mikroskopem [Analysis of STM images acquired by electron microscope]. Master's thesis, Charles University, Prague

Villarrubia JS (1997) Algorithms for scanned probe microscope image simulation, surface reconstruction, and tip estimation. J Res Natl Inst Stand Technol 102:102–425

Vincent L, Soille P (1991) Watersheds in digital spaces: an efficient algorithm based on immersion simulations. IEEE Trans Pattern Anal Mach Intell 13(6):583–598. doi:10.1109/34.87344

Vyňuchal J, Luňák S Jr, Hatlapatková A, Hrdina R, Lyčka A, Havel L, Vyňuchalová K, Jirásko R (2008) The synthesis, absorption, fluorescence and photoisomerisation of 2-aryl-4-arylmethylidene-pyrroline-5-ones. Dyes Pigment 77(2):266–276. doi:10.1016/j.dyepig.2007.05.001